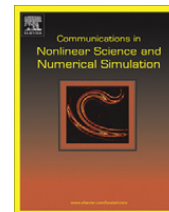




Contents lists available at ScienceDirect

Commun Nonlinear Sci Numer Simulat

journal homepage: www.elsevier.com/locate/cnsns

Internally cooled convection: A fillip for Philip

M. Berlingiero^a, K.A. Emanuel^b, J. von Hardenberg^a, A. Provenzale^{a,*}, E.A. Spiegel^c^aISAC-CNR, Torino, Italy^bEAPS-MIT, Cambridge, MA, USA^cDept. of Astronomy, Columbia University, New York, NY, USA

ARTICLE INFO

Article history:

Available online 22 July 2011

Keywords:

Convection

Numerical simulations

Geophysical fluid dynamics

ABSTRACT

We discuss a simplified mathematical description of internally cooled convection that includes a constant adiabatic lapse rate and an internal energy sink. The latter provides a representation of radiative cooling and, in combination, these two effects break the up-down symmetry of the vertical motions by making the convection penetrative in the upper portion of the fluid layer. At large enough turbulent intensity of the motion, the dynamics is dominated by intense convective updrafts that generate a strongly skewed distribution of vertical velocities. The numerical exploration of this model system exhibits a qualitatively useful description of atmospheric convection.

© 2011 Elsevier B.V. All rights reserved.

1. Introduction

The full physical description of atmospheric convection requires the use of a set of complex partial differential equations which include fluid dynamical, thermodynamical and microphysical effects [9,14,31]. Even the numerical solution of such equations is quite demanding, and the complications associated with their treatment could hamper basic understanding of issues related to linear stability, weakly nonlinear saturation, pattern formation and turbulent transport.

In the belief that simpler approaches to atmospheric convection can be used to gain some insight into its general behavior, we propose here a version of the equations that is amenable to modest numerical approaches and analytical study.

Our point of departure is a layer of incompressible fluid enclosed between two rigid parallel plates and heated from below, the standard known as Rayleigh–Benard (RB) convection. For this case there is available a range of analyses from linear stability theory [4], to nonlinear pattern formation studies [5], through the consideration of plume dynamics [33,19] and of turbulent transport [27]. The RB problem has become a paradigm of nonlinear science and much has been understood of its workings, though a complete picture of the fully turbulent regime is still lacking (as for most other turbulent flows).

Convection as observed in planetary atmospheres and in stars, on the other hand, is characterized by additional complications such as compressibility, rotation, phase transitions, magnetic fields and radiative effects. A full quantitative treatment of these systems requires careful detailed consideration of the additional effects. To begin to bridge the wide gap between the two manifestations of convection, it is useful to start from the base state of RB convection and add various special effects individually to ascertain what each may contribute to the general behavior. This approach has been well recognized for the case of many of the key effects. Here we consider the inclusion of a stand-in, a metaphor really, for radiative cooling in the form of a simple additional term in the heat equation. The resulting extension of RB convection produces flows that qualitatively resemble those of atmospheric convection.

* Corresponding author.

E-mail address: a.provenzale@isac.cnr.it (A. Provenzale).

The constant heat loss term representing radiative losses that we include in our equations would not make a great difference to the problem if we did not also include the adiabatic lapse rate (or gradient) in the heat equation. This is an effect that arises from even a slight compressibility of the fluid even though the motion may be treated as incompressible [16]. This is a subtle point over which much ink has been spilled and we shall not attempt to rehash that discussion. Suffice it to say that the adiabatic lapse rate has often been omitted from studies of RB convection. However, it is crucial to our study since the combined workings of the cooling term and the adiabatic lapse rate give rise to a layer in the fluid which is locally stable in the sense of linear theory. This effect is central in shaping the qualitative nature of the convective motions to be discussed below.

Of course, we are omitting most of the complicating effects; the Earth atmosphere is turbulent, radiatively active, non-Boussinesq, moist and precipitating, affected by large-scale shear flows, and subject to inhomogeneous boundary conditions, requiring the use of full non-hydrostatic moist convection models for a realistic description [9,22,31]. Of these omissions, the one most related to our present study is that this formulation does not contain any explicit moisture dynamics, a crucially important aspect of the real atmosphere which is overlooked here. Thus, the model we discuss is appropriate for a layer of moist air (as most of the radiative cooling comes from water vapor) which *never* gives rise to water condensation and precipitation.

The dynamics of a fluid layer with constant internal cooling has been recently addressed in other studies [12], albeit with a different perspective. Moreover, the model discussed here has an interesting dual formulation for a layer with constant internal heating, which is an approximate description of the dynamics of the Earth mantle where radioactive decay provides continuous internal heating [25].

The rest of this paper proceeds as follows. Section 2 gives a description of the mechanisms included in the model. In Section 3 we write the equations of motion. Section 4 is devoted to the properties of the static solution and its linear stability. In Section 5 we discuss the properties of the convection generated by the model in the fully nonlinear regime; in Section 6 we give conclusions and perspectives.

2. Ingredients of the model

A central ingredient of atmospheric convection is the forcing associated with the heat flux from the lower boundary due to warming of the Earth's surface by solar radiation. The heat flux from the lower boundary is usually carried by small-scale turbulent eddies. At the lower boundary we use a bulk formula relating the heat flux to the turbulent velocity, namely

$$-K_e \frac{\partial T}{\partial z} = c(T - T_{ground}), \quad (1)$$

where z points vertically upwards, T is temperature, K_e is eddy diffusivity, c is a turbulent velocity scale and T_{ground} is the temperature at the Earth's surface as determined by the incoming solar radiation and the surface albedo [9,22]. We shall further simplify this specification by assuming a fixed heat flux from the lower boundary, $\partial T/\partial z = \text{Const}$. The fixed-flux boundary conditions lead to different linear stability properties of the stationary state than the more usual fixed-temperature boundary conditions [13].

The study of radiative-convective systems has a long history in atmospheric dynamics and astrophysics [23,10,11,29,3,17,1], see also [30] and references therein for a recent review with a focus on geophysics. Here, however, we take an extremely simplified approach and represent the radiative loss from the atmosphere into space by including a constant loss term in the heat equation. The main effect of this constant cooling term is to provide an internal sink for mechanical and thermal energy, part of which is transformed into radiation which is assumed to escape from the system. (For previous explorations of atmospheric convection with prescribed internal radiative cooling see [6,15,24,18].) As mentioned above, this problem is formally equivalent, after the transformation $z \rightarrow -z$ and $T \rightarrow -T$, to the case of a fluid layer which is heated internally and cooled at the surface. A similar description has been used in the study of mantle convection [25].

The assumption of constant radiative cooling is drastic, and it does not do justice to the details of radiative convection. On the other hand, experimental data in strongly convective regions suggest that radiative cooling is approximately constant in extended regions of the troposphere; see [28] for a discussion of the results obtained during the GATE experiment. We adopt this view and include a constant radiative cooling in the model formulation. The constant radiative cooling changes the static profile of the convective fluid, but does not alter the structure of the temperature perturbations.

The constant thermal energy sink in concert with the adiabatic lapse rate breaks the up-down symmetry inherent in the Rayleigh–Benard problem. The latter is an additional aspect to be taken into account because of the thermal effects of work done by pressure forces in the convective process. Since the atmosphere is compressible, we need to introduce a dry adiabatic lapse rate generated by the compressibility of the static stratification. Despite this effect of compressibility, the Boussinesq approximation may be used for the density perturbations and incompressibility of the fluid velocity field may be assumed [16]. As we shall see below, the presence of this term leads to the convection being of penetrative type, and it naturally allows for the existence of a stably-stratified upper layer.

3. Equations of motion

The model considered here describes the motions taking place in a layer of air which is bounded above and below by two horizontal surfaces and is internally cooled by a constant radiative sink. Heat enters the system from the lower boundary, and it is transferred in the interior of the layer mainly by convection. Heat is lost from the system by radiation to outer space, and the upper boundary is assumed to be transparent to radiation. Molecular viscosity and heat conduction are neglected since the Rayleigh number is very large and the flow may be assumed to be fully turbulent.

Since we do not resolve the full spectrum of scales of motion, we include two terms parameterizing turbulent diffusion of momentum and heat. To this end, we use an elementary description of the unresolved dynamics and rely upon a simple eddy diffusion approach.

The equations of motion can then be expressed in non-dimensional form as:

$$\frac{D\mathbf{u}}{Dt} = -\nabla p + T\hat{\mathbf{z}} + \frac{\tau_c}{\tau_e} \nabla^2 \mathbf{u}, \quad (2)$$

$$\nabla \cdot \mathbf{u} = 0, \quad (3)$$

$$\frac{DT}{Dt} + \gamma w = -\frac{\tau_c}{\tau_{rad}} + \frac{\tau_c}{\tau_e} \nabla^2 T. \quad (4)$$

Here $\mathbf{u} = (u, v, w)$ is the fluid velocity, $\mathbf{x} = (x, y, z)$ is the spatial coordinate with z pointing upwards, $\hat{\mathbf{z}}$ is the unit vector in the vertical direction, t is time, p is pressure, T is temperature and $D/Dt = \partial/\partial t + \mathbf{u} \cdot \nabla$ is the material derivative. We have non-dimensionalized the spatial coordinate by the depth of the fluid layer, H , and time by the characteristic time $\tau_c = (\alpha T_0 g/H)^{-1/2}$ where T_0 is a temperature scale to be chosen below, α is the coefficient of thermal expansion and g is the acceleration of gravity. The density perturbation is determined entirely by the temperature perturbation (i.e., pressure affects only the density profile of the hydrostatic solution). The term γw is owing to the pressure dependence of the hydrostatic profile. Here $\gamma = \Gamma H/T_0$ where Γ is the dimensionful adiabatic lapse rate, equal to g/c_p for unsaturated air, where c_p is the specific heat at constant pressure, and lower for saturated air.

In the above equations we have represented viscous and thermal diffusion by turbulence at unresolved scales by a simple eddy diffusion closure. We have assumed the same timescale, $\tau_e = H^2/K_e$ where K_e is the eddy diffusivity, for the turbulent diffusion of momentum and heat (that is, we assumed an effective Prandtl number $\sigma = 1$). On the scales of interest, turbulent diffusion is paramount and molecular diffusion is negligible. From the different time scales we can define an effective Reynolds number, $Re = \tau_e/\tau_c$, and an effective Rayleigh number, $Ra = \tau_e^2/\tau_c^2 = Re^2$.

The first term on the right-hand-side of the thermodynamic equation is the non-dimensional representation of a constant radiative cooling. The dimensionful formulation of radiative cooling includes the negative of the divergence of the dimensionful radiation flux, $J_0 = \tilde{\nabla} \cdot \mathbf{F}$. That is

$$\tilde{D}\tilde{T}/\tilde{D}\tilde{t} + \Gamma\tilde{w} = -J_0/(\rho c_p) + K_e \tilde{\nabla}^2 \tilde{T}. \quad (5)$$

The tildes on T , \mathbf{u} and their derivatives indicate that these are dimensionful variables. The radiative flux, \mathbf{F} , should in principle be determined by an equation describing radiative effects. We have assumed that the radiative flux responsible for cooling the air is a linear function of height, a choice which gives a constant value of J_0 . The quantity $\tau_{rad} = \rho c_p T_0/J_0$ is the time scale of radiative cooling. We can also define a radiative Rayleigh number, $Ra_{rad} = \tau_e \tau_{rad}/\tau_c^2$, which is the appropriate control parameter when the principal heat sink is radiative cooling.

For the application of the boundary conditions, we assume that the fluid layer is bounded above and below by the planes at $z = 0, 1$, where either no-stress or no-slip conditions on velocity are imposed. As stated, heat enters the system from below at a prescribed, constant heat flux at the lower surface: $-\partial T/\partial z = f_0$ at $z = 0$ ($f_0 > 0$). The heat entering from below is partly lost inside the fluid layer through radiative losses into space. The heat that is not lost through radiation is assumed to escape from the upper boundary with a constant heat flux: $-\partial T/\partial z = f_1 \leq f_0$ at $z = 1$.

The requirement of (statistical) radiative-convective equilibrium implies a balance between input and output heat fluxes. Averaging the equations in space and time leads to the requirement $f_0 = f_1 + \tau_e/\tau_{rad}$. If radiative effects are unimportant, $\tau_{rad} \rightarrow \infty$ and the system becomes a standard fixed-flux RB setting (with or without an adiabatic lapse rate term). Another case of interest, which will be considered in detail in the following, is when all heat is lost to radiation from inside the fluid layer, and the upper boundary is transparent to radiation but thermally insulating. In this case one has $f_1 = 0$ and $f_0 = \tau_e/\tau_{rad}$.

At this point, we still have the freedom of choosing the temperature perturbation scale, T_0 . In standard fixed-temperature Rayleigh-Benard convection, the temperature scale is dictated by the temperature difference between the two plates. Here, we define the temperature scale T_0 by requiring that $\tau_c = \tau_{rad}$, which gives $T_0 = [HJ_0^2/(g\alpha\rho^2 c_p^2)]^{1/3}$ and defines the velocity scale as $U = H/\tau_c = (gJ_0 H^2/\rho c_p T_0)^{1/3}$. In this way, $Ra_{rad} = \tau_e/\tau_c = Re$, and the lower boundary condition becomes $f_0 = Ra_{rad}$. With this formulation, the system has two free parameters, namely the radiative Rayleigh number (or equivalently, the effective Reynolds number) and the adiabatic lapse rate, γ . The choice of T_0 adopted here does not allow for taking the limit $\tau_{rad} \rightarrow \infty$ so that this is not a good scaling for studying the transition to convection without radiative cooling.

4. Static solution

With the radiative cooling associated to a finite value of τ_{rad} , system (1–3) has a static solution with $\mathbf{u} = 0$ and temperature depending quadratically on height, $T_s(z) = -Ra_{rad}z(1 - z/2)$ where we have set $T_s(0) = 0$, without loss of generality. The quadratic form of the static solution is independent of the value of the adiabatic lapse rate γ . (Without the cooling term and with boundary conditions $f_0 = f_1$, the static state has a linear profile in z). The cooling term also breaks the up-down symmetry of RB convection, namely invariance of the equations under the transformation $T \rightarrow -T$, $w \rightarrow -w$ and $z \rightarrow -z$.

The presence of the adiabatic lapse rate adds a further element to the dynamics since the stability of the static state depends on the value of γ . When the adiabatic lapse rate term is absent, one gets the equivalent of the standard fixed-flux, long-wavelength instability encountered in Rayleigh–Benard convection with fixed-flux boundary conditions. In that case the critical horizontal wavenumber of the convection is zero. When $\gamma \neq 0$, however, the first instability is encountered at finite wavenumber, similarly to what is observed in compressible convection [7] and in weakly non-Boussinesq convection [8]. The critical (effective) radiative Rayleigh number for instability and the critical wavenumber both grow with γ . See [17,1] for further details on the linear stability of the static state in radiative-convective fluid layers, and [26] for a study of the linear stability of mildly penetrative convection.

5. Strongly nonlinear dynamics

5.1. Procedure

At values of the radiative Rayleigh number well above critical, the convective motion becomes irregular. Also in this regime, wherever $dT_s/dz \geq -\gamma$, the static state is hydrostatically stable locally. For any finite value of γ , the quadratic form of T_s ensures the existence of a stable upper layer for $z_0 \leq z \leq 1$, where $z_0 = 1 - \gamma/Ra_{rad}$. In such conditions, convection becomes penetrative, and it is characterized by overturning motions below a stable upper layer where internal waves are continuously excited by the convection below. The presence of the adiabatic lapse rate alone is not enough to generate penetrative convection since the static profile is linear when there is no radiative cooling. For a linear static profile and a constant adiabatic lapse rate, the layer is either all stable or all unstable with no variation in local stability. These are known effects, which the simplicity of our model allows us to elucidate. This we do with a numerical exploration of the system's behavior.

For the numerical simulation of the model (1–3) we adopt a code that is a modification of a pre-existing 3D spectral-finite difference Navier–Stokes solver, see [21,19] and references therein for a description of the numerical code and its validation on known conditions. The code is spectral in the horizontal, with 4/5 dealiasing, finite differencing in the vertical, and resolution of 192^2 grid points in the horizontal and 129 (unequally-spaced) points along the vertical. Time advancement is by a third-order fractional step method. The simulations considered here have periodic boundary conditions in the horizontal and the simulation box has non-dimensional size $(2\pi, 2\pi)$. Here we report on simulations for the case $Re = Ra_{rad} = 300$. That is, $Ra = 9 \times 10^4$ and $\gamma = 100$, which gives $z_0 = 2/3$ so that the upper third of the fluid layer is statically stable (locally).

For the initial conditions we use a random perturbation of the static state $T_s(z)$. After an initial transient, which is excluded from the results reported below, the system settles to a state of statistical radiative-convective equilibrium. In dimensionful

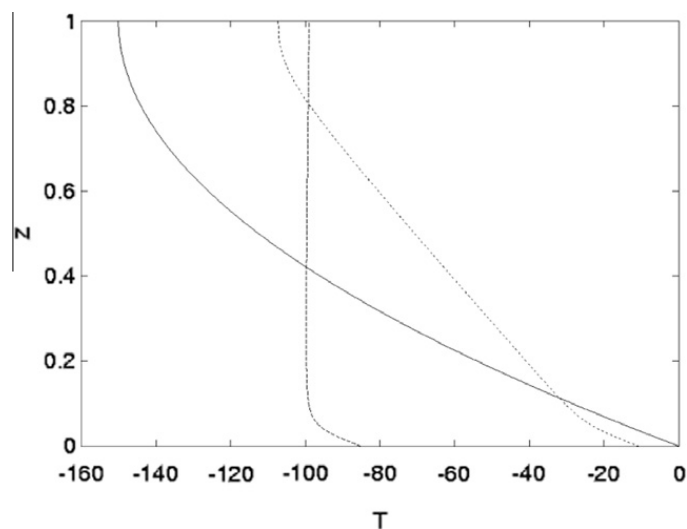


Fig. 1. Temperature profiles as a function of height, z . Solid curve: temperature profile for the (unstable) static state. Dotted curve: horizontally and temporally averaged temperature profile for $Ra_{rad} = 300$, $\gamma = 100$. Dashed curve: horizontally and temporally averaged temperature profile for $Ra_{rad} = 300$, $\gamma = 0$.

variables, this configuration corresponds to simulating a layer of atmosphere with thickness of about 1000–3000 m, depending on the values assumed for the adiabatic lapse rate and the cooling rate.

5.2. Results

Fig. 1 shows the temperature profile of the static state, $T_s(z)$, compared with the horizontally and temporally averaged temperature profiles, $\bar{T}(z)$, obtained at $Ra_{rad} = 300$ with and without the adiabatic lapse rate. In convective equilibrium, these profiles show that the convective mixing above the diffusion-dominated bottom boundary layer pushes the average temperature profile towards a state of neutral hydrostatic stability. When $\gamma = 0$, the fluid interior above the bottom boundary layer becomes isothermal. When $\gamma \neq 0$, the convective mixing brings the temperature profile to the linear, neutrally stable profile with $d\bar{T}/dz = -\gamma$. As discussed above, for $\gamma \neq 0$ the convecting system displays a hydrostatically stable upper layer where the profile remains close to that of the static state. Moreover, the stable layer appears slightly above $z_0 = 2/3$ as the penetrating convective motions erode its lower portion.

The mixing of the fluid core between the bottom boundary layer and the stable layer above is caused by the action of an ensemble of coherent convective plumes. However, when internal cooling and a non-zero adiabatic lapse rate are present, only strong ascending coherent plumes are observed, in qualitative agreement with what is observed in atmospheric

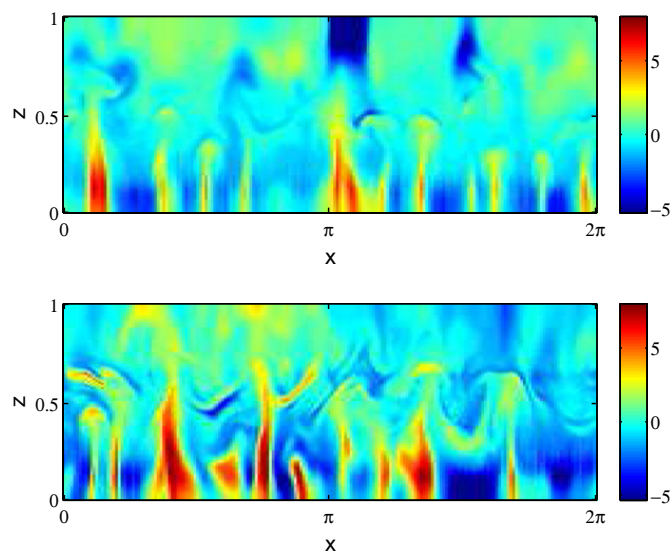


Fig. 2. Vertical slices of the instantaneous temperature perturbation field at $t = 40$, after statistical equilibrium has been reached, for $Ra_{rad} = 300$ and $\gamma = 100$ (upper panel), and for $Ra_{rad} = 300$ and $\gamma = 0$ (lower panel).

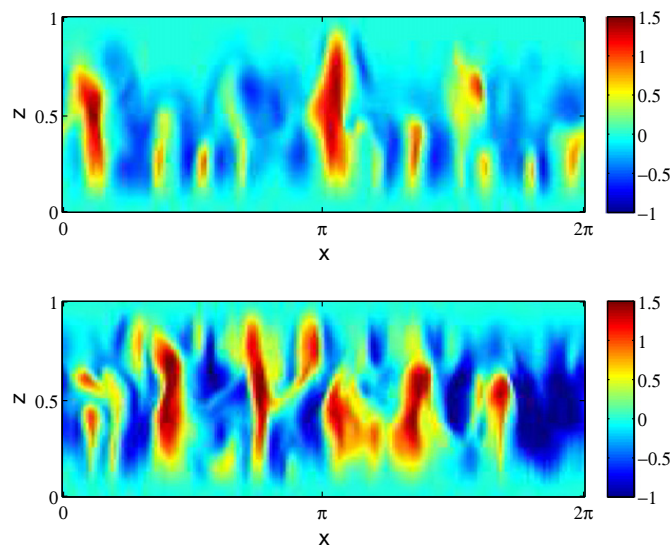


Fig. 3. Vertical slices of the instantaneous vertical velocity field at $t = 40$, after statistical equilibrium has been reached, for $Ra_{rad} = 300$ and $\gamma = 100$ (upper panel), and for $Ra_{rad} = 300$ and $\gamma = 0$ (lower panel).

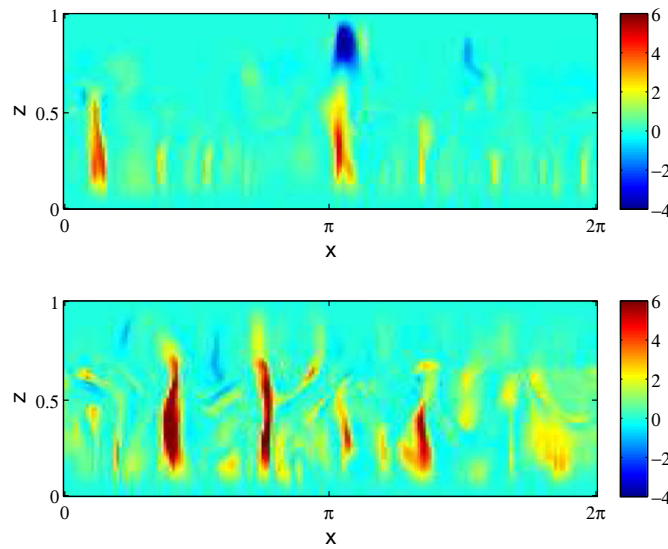


Fig. 4. Vertical slices of the instantaneous convective heat flux field at $t = 40$, after statistical equilibrium has been reached, for $Ra_{rad} = 300$ and $\gamma = 100$ (upper panel), and for $Ra_{rad} = 300$ and $\gamma = 0$ (lower panel).

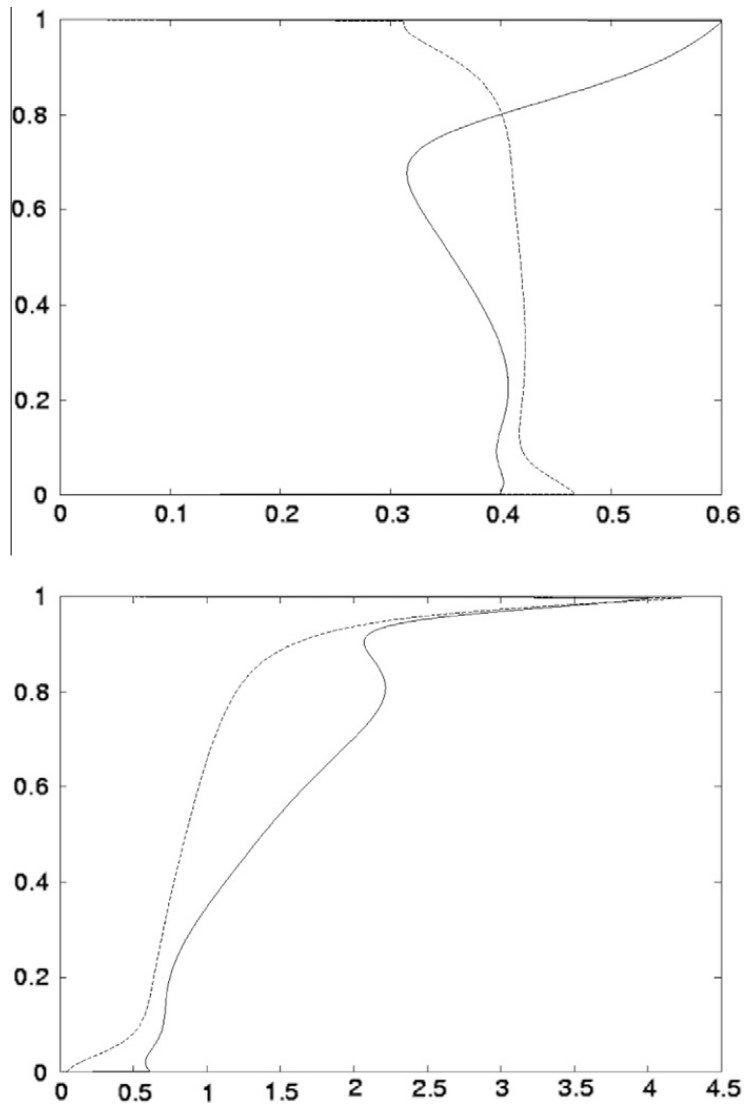


Fig. 5. Vertical profiles of the temporally averaged fraction of horizontal area occupied by upward velocities (upper panel) and skewness of the vertical velocities (lower panel). Solid curves correspond to $Ra_{rad} = 300$, $\gamma = 100$, dashed curves correspond to $Ra_{rad} = 300$, $\gamma = 0$.

convection [9]. Figs. 2–4 show slices of the temperature perturbation, of the vertical velocity and of the convective heat flux, defined as $w[T - \bar{T}(z)]$, after the statistical convective equilibrium has been attained, for $Ra_{rad} = 300$ and $\gamma = 100$ (upper panels) and for $\gamma = 0$ (lower panels). The plumes originate in the lower boundary layer and bring warm fluid to the top of the convecting layer. The local temperature perturbations and the vertical velocities are intense in the plumes, which are effective transporters of heat. When $\gamma \neq 0$, we observe the additional effect of a stable layer above the convectively unstable fluid, where temperature perturbations propagate horizontally without giving rise to convection.

The asymmetry between updrafts and downdrafts is reflected in the statistics of vertical velocities. Fig. 5a shows the vertical profile of the temporally averaged fraction of horizontal area characterized by upward velocities, for the case $\gamma = 100$ (solid line) and for $\gamma = 0$ (dashed line). With the adiabatic lapse rate, about 40% of the horizontal area is occupied by positive vertical velocities, in agreement with the observed behavior of atmospheric convection in the planetary boundary layer [32]. Without the adiabatic lapse rate term, the convection ceases to be penetrative and the asymmetry between updrafts and downdrafts is reduced.

Fig. 5b shows the vertical profile of the skewness of the distribution of vertical velocities. For $\gamma = 100$, the skewness is positive and it grows with height, again in agreement with atmospheric observations [32]. By contrast, vertical velocities have zero skewness in RB convection and they are much less skewed when the adiabatic lapse rate term is absent. When there is no adiabatic lapse rate term, the plumes impinging on the upper plate generate strong return downward flows, which are absent when the adiabatic lapse rate is included. When $\gamma \neq 0$, the fluid descends downwards with a slow and extended

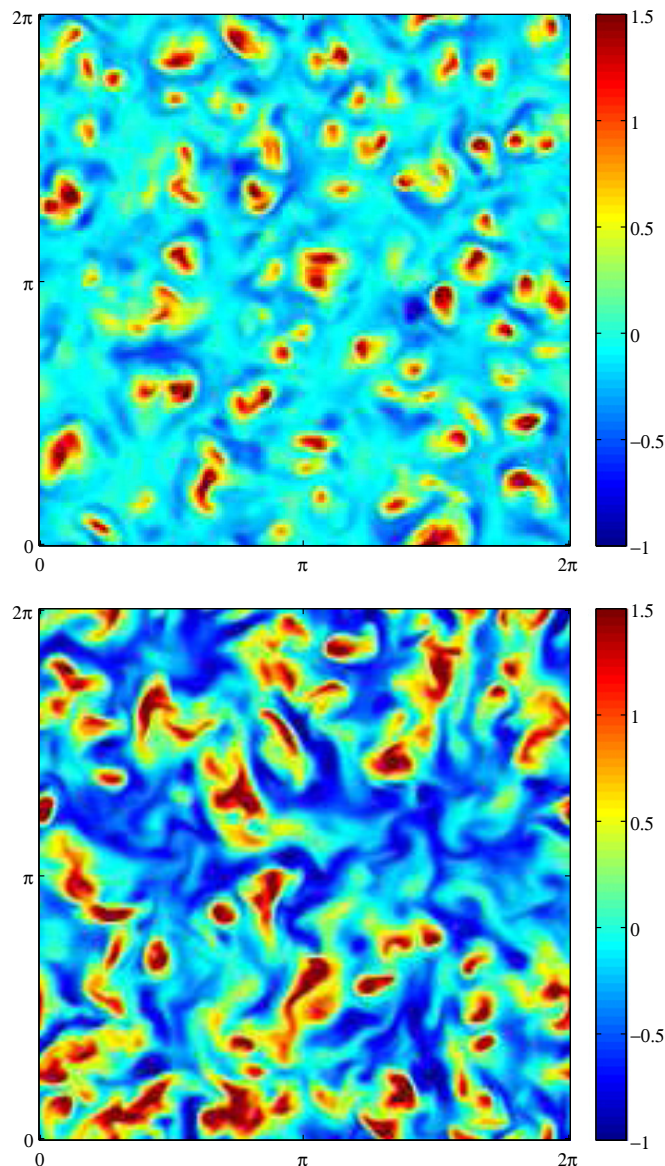


Fig. 6. Horizontal slices of the vertical velocity at $z = 0.68$ (at the top of the convecting layer) and time $t = 40$, well into the statistical stationary regime after the initial transient, for $Ra_{rad} = 300$ and $\gamma = 100$ (upper panel) and $\gamma = 0$ (lower panel).

motion. These results indicate that even a simple physical model like that discussed here can reproduce some of the basic properties of the convective atmosphere.

5.3. A remark

In Rayleigh–Benard convection with boundary conditions periodic in the horizontal directions, numerical simulations show that plumes undergo a clustering process as a result of which plumes form aggregates on scales containing many plumes (see [19,20] and references therein). We may then ask whether such a process is active also in the internally-cooled convective fluid studied here.

We observed a similar clustering effect when the adiabatic lapse rate is omitted ($\gamma = 0$). When an adiabatic lapse rate term is included, however, no plume clustering is observed. Fig. 6 shows two horizontal slices of the vertical velocity at $z = 0.68$ (at the top of the convecting layer) for the cases $\gamma = 100$ (upper) and $\gamma = 0$ (lower), at $t = 40$, after the initial transient has died out and the system entered a statistically-stationary regime. Fig. 7 shows the temperature perturbation close to the layer bottom at $z = 0.14$, where the plume roots are located, for the case $\gamma = 100$ (upper) and $\gamma = 0$ (lower) at $t = 40$. Plume clustering for $\gamma = 0$ is evident. For $\gamma = 100$, the individual plumes display an approximately homogeneous distribution.

This result is consistent with the conjecture offered in [19] that plume clustering is a result of the interaction of strong updrafts and downdrafts impinging on the boundary layer opposed to that where they were generated. In this picture, the

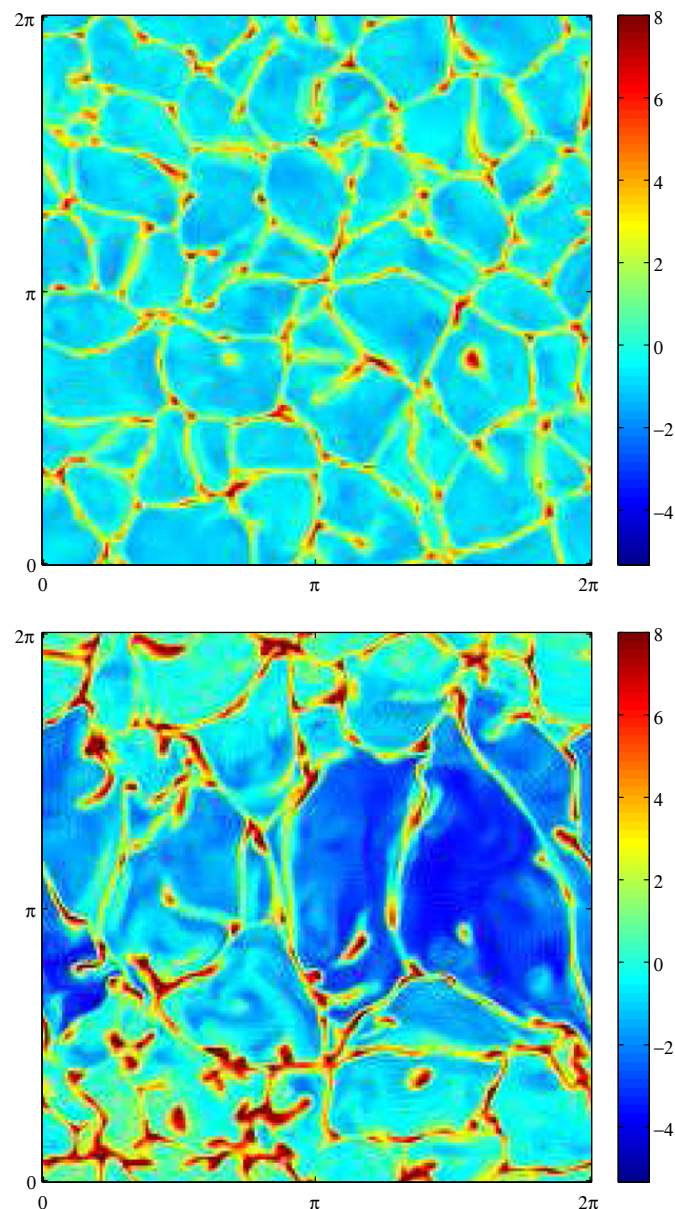


Fig. 7. Horizontal slices of the temperature perturbation at $z = 0.14$ (close to the layer bottom) and time $t = 40$, well into the statistical stationary regime after the initial transient, for $Ra_{rad} = 300$ and $\gamma = 100$ (upper panel) and $\gamma = 0$ (lower panel).

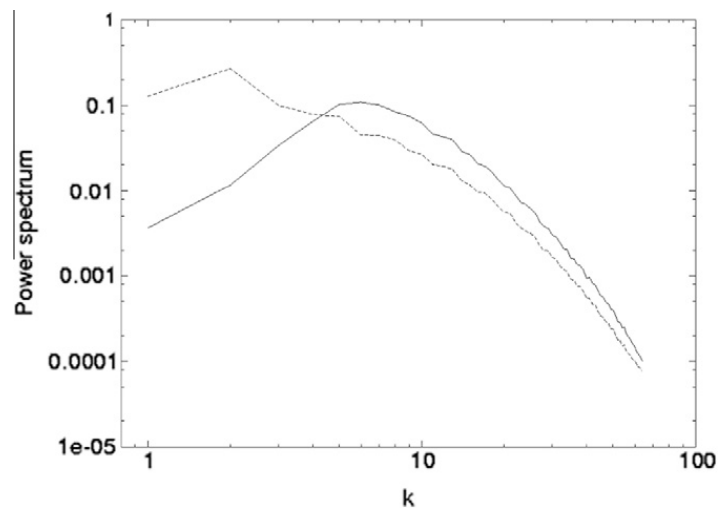


Fig. 8. Power spectrum as a function of the horizontal wavenumber k at $z = 0.68$, for the case $Ra_{rad} = 300$ and $\gamma = 100$ (solid line) and for $\gamma = 0$ (dashed line). Without the adiabatic lapse rate term, the spectral power is peaked at low wavenumber due to a process of plume clustering. The spectra have been temporally averaged over several characteristic times in the statistically-stationary regime.

impinging plumes generate horizontally divergent flows in the boundary layer that they hit, pushing the roots of newly forming plumes close to each other and eventually leading to plume clustering.

A similar process occurs here for the case $\gamma = 0$. Even though in this case there are no *bonafide* descending coherent plumes, the downdrafts are nevertheless quite intense, as shown by the small skewness of the vertical velocity distribution. On the other hand, when an adiabatic lapse rate is included, the plumes are prevented from reaching the opposite boundary, and no interaction between hot plumes and the upper boundary layer takes place. In this case, the return flow is very weak, and the clustering of plumes is not observed. Two spatial scales are then present, namely, the size of the individual plumes, and the mean inter-plume distance.

Fig. 8 shows the power spectra as functions of the horizontal wavenumber for the two cases with and without the adiabatic lapse rate, at a late time well after statistical radiative-convective equilibrium has been reached. When $\gamma = 0$, the spectrum is maximum at low wavenumbers, consistent with the presence of plume clustering and indicating that the system is dominated by a large-scale flow at the scale of the simulation box adopted here. Conversely, when $\gamma \neq 0$ the spectrum is peaked at intermediate wavenumbers, consistently with the absence of plume clustering. The spectral peak measures, in this case, the size of the mean inter-plume distance.

6. Summary and conclusions

In this work we have discussed a simple mathematical description of internally cooled convection. The description includes a constant heat flux from the lower boundary, an internal constant energy sink meant to represent radiative cooling, and an adiabatic lapse rate. It is meant as a prelude to a more extensive study of atmospheric convection when the thermodynamic effects of water vapor condensation are not essential to the description, as in the case of sub-saturated air or for non-precipitating moist air when evaporation and condensation balance.

In the fully nonlinear regime, we observed that the flow is characterized by the presence of intense updrafts and a weak downward return flow, consistent with the behavior of atmospheric convection. Such non-Boussinesq asymmetry is also observed in the study of fully compressible convection [2]. We have also confronted the dynamics that are obtained with and without an adiabatic lapse rate, showing that different large-scale properties emerge in the two cases.

The picture introduced here is not meant to provide a detailed representation of atmospheric convection, for which much more complex models need to be adopted [9,31]. The virtue of our simplified approach is that it can capture salient features of atmospheric convection while including only some of the basic physical ingredients of the system and remaining analytically tractable (at least at the linear and weakly nonlinear level). We hope that our birthday celebrant enjoys the pictures.

References

- [1] Aumaître S. Radiative convection with a fixed heat flux. *Physica D* 2001;158:164–74.
- [2] Cattaneo F, Brummell NH, Toomre J, Malagoli A, Hurlburt NE. Turbulent compressible convection. *Astrophys J* 1991;370:282–94.
- [3] Chandrasekhar S. Radiative transfer. New York: Dover; 1960.
- [4] Chandrasekhar S. Hydrodynamic and hydromagnetic stability. New York: Clarendon Press; 1968.
- [5] Cross MC, Hohenberg PC. Pattern formation outside of equilibrium. *Rev Mod Phys* 1993;65:851–1112.
- [6] Deardorff JW. Numerical investigation of neutral and unstable planetary boundary layers. *J Atmos Sci* 1971;29:91–115.
- [7] Depassier MC, Spiegel EA. The large-scale structure of compressible convection. *Astron J* 1981;80:496–512.

- [8] Depassier MC, Spiegel EA. Convection with heat flux prescribed on the boundaries of the system. I: The effect of temperature dependence of material properties. *Geophys Astrophys Fluid Dyn* 1982;21:167–88.
- [9] Emanuel KA. *Atmospheric convection*. New York: Oxford University Press; 1994.
- [10] Goody RM. The influence of radiative transfer on cellular convection. *J Fluid Mech* 1956;20:424–35.
- [11] Goody RM. *Atmospheric radiation*. Oxford: Oxford University Press; 1964.
- [12] Hartlep T, Busse FH. Convection in an internally cooled fluid layer heated from below, center for turbulence research, annual research briefs 2006,2006;355–362.
- [13] Hurle DTJ, Jakeman E, Pike ER. On the solution of the Benard problem with boundaries of finite conductivity. *Proc R Soc London A* 1967;296:469–75.
- [14] Houze Jr RA. *Cloud dynamics*. San Diego: Academic Press; 1993.
- [15] Islam S, Bras RL, Emanuel KA. Predictability of mesoscale rainfall in the tropics. *J Appl Meth* 1993;32:297–310.
- [16] Jeffreys. The instability of a compressible fluid heated below. *Proc Cambridge Phil Soc* 1930;26:170–2.
- [17] Larson VE. The effects of thermal radiation on dry convective instability. *Dyn Atmos Oceans* 2001;34:45–71.
- [18] Parodi A, Emanuel KA, Provenzale A. Plume patterns in radiative-convective flows. *New J Phys* 2003;5:106.1–106.17.
- [19] Parodi A, von Hardenberg J, Provenzale A, Spiegel EA. Clustering of plumes in turbulent convection. *Phys Rev Lett* 2004;92:194503.
- [20] Parodi A, von Hardenberg J, Provenzale A, Spiegel EA. Large-scale patterns in Rayleigh-Bénard convection. *Phys Lett A* 2008;372:2223–9.
- [21] Passoni G, Alfonsi G, Galbiati M. Analysis of hybrid algorithms for the Navier–Stokes-equations with respect to hydrodynamic stability theory. *Int J Numer Method Fluids* 2002;38:1069–89.
- [22] Pielke RA. *Mesoscale meteorological modeling*. 2nd ed. Academic Press; 2002 [International Geophysics Series].
- [23] von Prandtl L. Eine Beziehung zwischen Wärmeaustausch und Strömungswiderstand der Flüssigkeiten. *Physica Z* 1910;XI:1072–8.
- [24] Robe F, Emanuel KA. Moist convective scaling: some inferences from three-dimensional cloud ensemble simulations. *J Atmos Sci* 1996;53:3265–75.
- [25] Roberts PH. Convection in horizontal layers with internal heat generation. *Theor J Fluid Mech* 1967;30:33–49.
- [26] Roberts AJ. An analysis of near-marginal, mildly penetrative convection with heat flux prescribed on the boundaries. *J Fluid Mech* 1985;158:71–93.
- [27] Siggia ED. High Rayleigh number convection. *Ann Rev Fluid Mech* 1994;26:137–68.
- [28] Smith WL, Shen WC, Howell HB. A radiative heating model derived from the GATE MSR experiment. *J App Method* 1977;16:384–92.
- [29] Spiegel EA. The convective instability of a radiating fluid layer. *Astrophys J* 1960;132:716–28.
- [30] Spiegel EA. An introduction to radiative transfer for geophysicists. In: Weiss JB, Provenzale A, editors. *Transport and mixing in geophysical flows*. Lecture notes in physics. Berlin: Springer; 2008.
- [31] Stevens B. Atmospheric moist convection. *Ann Rev Earth Planet Sci* 2005;33:605–43.
- [32] Stull RB. *An introduction to boundary layer meteorology*. New York: Springer; 2004.
- [33] Turner JS. *Buoyancy effects in fluids*. Cambridge, UK: Cambridge University Press; 1973.